A WEIGHTED IMPLICIT FINITE VOLUME MODEL FOR OVERLAND FLOW

A. M. Wasantha Lal, [1], M. ASCE

A weighted implicit finite volume model is developed to simulate two dimensional diffusion flow in arbitrarily shaped areas. The model uses a mixture of unstructured triangles and quadrilaterals to discretize the domain, and a mixture of cell wall types to describe structures, levees, and flow functions that characterize two dimensional flow. The implicit formulation makes the model stable and run faster with very large time steps. The sparse system of linear equations that result from the implicit formulation is solved by using iterative solvers based on various pre-conditioned conjugate gradient methods. The model was tested under a variety of conditions. The results were compared to results from known models applied to axisymmetric and other test problems that had known solutions.

The model was successfully applied to the Oxbow section of the Kissimmee River in Florida, and the results were compared with results from physical and numerical modeling studies. This analysis indicated that the circumcenter-based flow function for walls that is used in the model gives overall superior results in all the cases considered. Results of the numerical experiments showed that the use of weighted implicit methods and iterative solvers provide modelers with improved flexibility and control of the overall accuracy and the run time. The method is to be used as an efficient solution method for local and regional modeling problems in South Florida.

INTRODUCTION

Simulation of overland flow is an important function of large scale hydrologic models. Many such models, including the NSM (Natural System Model) and the SFWMM (South Florida Water Management Model), which are used to simulate the hydrology of South Florida, are based on solving

[1]Lead Civil Engineer, South Florida Water Management District, 3301 Gun Club Rd., West Palm Beach, FL 33406

approximate forms of the St. Venant equations to simulate overland flow. An ideal model for the simulation of 2-D overland flow is expected to handle water bodies of arbitrary shape and may have to use a wide range of temporal and spatial features to meet accuracy requirements at different locations and times. Some of the historic developments related to this goal are described in the texts by Abbott (1979), Tan (1992), and Chaudhry (1993). The features that make models useful for practical applications include the ability to handle wetting and drying; the ability to simulate flow through structures such as weirs, gates and culverts; and the ability to handle tributary and slough inflows.

The earliest 2-D models to solve the St. Venant equations were based on various explicit finite difference methods and rectangular grids. Liggett and Woolhiser (1967), Chow and Ben-Zvi (1973), and Katopodes and Strelkoff (1978) developed some of the early models. More recently, complete equation models have been developed that are capable of handling the inertia terms better and can produce better results for dam-break types of dynamic problems. Fennema and Chaudhry (1990) and Garcia and Kahawita (1989) have developed two such models. Finite element and finite volume methods are useful when the flow domain is arbitrary and the discretization is non-uniform. Fenner (1975) and Akanbi and Katopodes (1988) developed models based on the finite element method, and Zhao et al. (1994) used a finite volume method for solving the complete equations. Most of the complete equation models that use irregular grids require a long time to run and are inefficient to use in large scale hydrologic applications, such as modeling of the Everglades, in which the inertia term is negligible. The challenge of maintaining both fine spatial resolution and low run times can be met by using diffusion flow models in which the inertia terms are neglected. In diffusion flow models one equation is solved for the water level, instead of the three coupled equations that form the St. Venant equations.

Ponce et al. (1978) established a theoretical range of applicability for diffusion flow models. Such models have been applied in the past by Xanthopoulos and Koutitas (1976) to simulate flood wave problems, by Akan and Yen (1981) to study channel confluence flow problems and by

Hromadka et al. (1985) to study dam failure problems. These studies showed that diffusion flow models can be used successfully to simulate a variety of natural flow conditions. Hromadka et al. (1987) also used a 2-D diffusion flow model to compare overland flow models. Diffusion flow models have been used successfully to simulate hydrologic conditions in the Everglades, using the NSM and the SFWMM models developed by the South Florida Water Management District (Fennema et al. 1994).

A finite volume method is useful for South Florida because many of the post-drainage features in the area take the shape of polygons bounded by levees and canals. It satisfies strict mass balance because of conservative property. The basic idea behind the finite volume method is to begin with the conservative form of the differential equation, integrate it over a finite volume, and use Gauss' theorem to convert results into surface integrals which can then be discretized (Hirsch, 1988). During the computation of these surface integrals along the cell walls, functions defining average wall fluxes are needed. Two types of functions are used in this paper, one which uses a line integral, and one which uses the circumcenters (centers of the circumscribing circles) of triangles. In the case of structures or any other flow features, these wall functions are replaced with appropriate functions. When a cell-centered finite volume method is used with rectangular grids, the finite volume method collapses to a finite difference method.

The ordinary differential equations resulting from the finite volume formulation can be solved by using a weighted implicit method. The weighting factor that is used in many 1-D models such as DAMBRK (Fread, 1973, 1988) provides control over accuracy and stability, and the weighting also makes it possible to produce solutions even under stiff conditions. The final solution of the finite volume method is the solution of a sparse system of linear equations at every time step. The availability of a variety of sparse solver methods and packages has made it possible to exercise control over the run time and accuracy.

Both direct and iterative methods are available to solve sparse systems. Iterative methods, such

as the preconditioned conjugate gradient method, are less susceptible to round-off error, and they are more efficient for large problems (Aziz and Settari, 1979). Some of the public domain sparse solvers available through the Internet include SLAP (Seager, 1988), Templates (Barrett, 1993) and IML++ (Dongarra, 1995). Numerous pre-conditioners are used with sparse solvers to speed convergence and sometimes to make the solution feasible. When flow conditions are nearly steady due to negligible disturbances from rainfall and other events, iterative solvers need very few iterations. This feature can make the current model run extremely fast except during unsteady events.

Hydrologic models applied to the South Florida landscape are expected to simulate both large-scale flow features in the Everglades and small-scale flow features in urban areas. They are expected to be capable of both long and short term simulations with relatively short run times. This paper describes the formulation, numerical testing, numerical error analysis, and the successful application of the model to a portion of the Kissimmee river. A number of additional tests were conducted to study the variation in numerical error with spatial and temporal discretizations. Results demonstrate the fast performance of the model when compared to explicit models. The results are also useful in selecting the spatial and temporal discretization for future applications of the model to other areas in South Florida. Some results shown at low resolutions give additional information about the behavior of numerical errors in the model output.

GOVERNING EQUATIONS

Overland flow is described by the depth-averaged flow equations commonly referred to as Saint Venant equations. These equations consist of a continuity equation and momentum equations. The two dimensional continuity equation for shallow water flow is

$$\frac{\partial h}{\partial t} + \frac{\partial (hu)}{\partial x} + \frac{\partial (hv)}{\partial y} - RF + IN + ET + q_{ea} = 0 \tag{1}$$

in which u and v are velocities in x and y directions; $h =$ water depth in units L; $RF =$ rainfall intensity; $IN =$ infiltration rate; $ET =$ evapotranspiration rate, all in units L/T; $q_{ea} =$ volume rate of overland flow entering or leaving canals, measured per unit cell area per unit time. The

momentum equations used in the x and y directions are

$$\frac{\partial(hu)}{\partial t}+\frac{\partial(u^2h)}{\partial x}+\frac{\partial(uvh)}{\partial y}+hg\frac{\partial(h+z)}{\partial x}+ghS_{fx}=0 \tag{2}$$

$$\frac{\partial(hv)}{\partial t}+\frac{\partial(uvh)}{\partial x}+\frac{\partial(v^2h)}{\partial y}+hg\frac{\partial(h+z)}{\partial y}+ghS_{fy}=0 \tag{3}$$

in which S_{fx} and $S_{fy}=$ components of friction slopes in x and y directions. The momentum equations can be combined with the continuity equation without the source term to produce the following vector momentum equation

$$\frac{\partial \mathbf{V}}{\partial t}+\nabla(\frac{1}{2}V^2+gH)+g\vec{S}_f+\mathbf{V}\times\omega=0 \tag{4}$$

in which $\omega=\nabla\times\mathbf{V}$; $\mathbf{V}=u\mathbf{i}+v\mathbf{j}=$ velocity vector; $\vec{S}_f=$ friction slope vector; $H=h+z=$ water level above the datum; $z=$ bottom elevation above datum. The steps in obtaining the equation are presented by Panton (1984). Equation (4) can be integrated along a stream line to obtain the commonly used energy equation. The first term in (4) which is the local acceleration term and the second term which is the convective acceleration term are responsible for inertia effects. The first term is neglected in slowly varying flow to obtain diffusion flow equations. If flow is irrotational, $\omega=0$ and (4) reduces to

$$\nabla E=-\vec{S}_f \tag{5}$$

which can also be written in terms of the x and y components as $\frac{\partial E}{\partial x}=-S_{fx}$ and $\frac{\partial E}{\partial x}=-S_{fy}$ with $E=h+z+V^2/(2g)=H+V^2/(2g)$ being the energy head above the datum. Equation (5) without the velocity head in E is normally used as the foundation of diffusion flow formulations, in which the water level H is used instead of the energy head E (Hromadka et al., 1987). Even if all of the equations that follow are expressed in terms of H, it can be shown that H in these equations can be replaced with E to give the necessary equations for conditions under which the velocity heads are important. This simple conversion is possible in slowly varying flow if $\frac{\partial}{\partial t}(V^2/2g)$ is small. Use of E instead of H helps to recover some of the lost inertia effects in slowly varying diffusion flow at converging and diverging boundaries. Unfortunately, diffusion flow models using the velocity head generate small oscillations in unsteady flow problems (Strelkoff et al., 1977), and it becomes

necessary to use H instead of E for such problems.

The friction slope $\vec{S}_f$ in (5) is computed using an equation for wetlands (Kadlec and Knight, 1996) or a general form of the Manning equation written as $V = \frac{1}{n_b} h^{\gamma} S_f^{\lambda}$ in which n_b = Manning coefficient when $\gamma = 2/3$ and $\lambda = 1/2$; $V = \sqrt{v^2 + u^2}$ = magnitude of the velocity vector. In diffusion flow $S_f = S_n$ is assumed, in which S_n = slope of the water surface (or the energy surface when E is used) computed as $\sqrt{(\frac{\partial H}{\partial x})^2 + (\frac{\partial H}{\partial y})^2}$. Akan and Yen (1981) and Hromadka et al. (1987) used the following equation to compute u and v:

$$u = -\frac{K}{h}\frac{\partial H}{\partial x}, \qquad v = -\frac{K}{h}\frac{\partial H}{\partial y} \tag{6}$$

K can be expressed for the Manning equation in general form as

$$K = \frac{1}{n_b} h^{\gamma+1} S_n^{\lambda-1} \quad \text{for} \quad \lambda \geq 1 \quad \text{and} \quad |S_n| > \delta_s \tag{7}$$

$$K = K_0 \quad \text{for} \quad \lambda < 1 \quad \text{and} \quad |S_n| \leq \delta_s \tag{8}$$

Term $K_0 = h^{\gamma+1}/(n_b \delta_s^{1-\lambda})$ provides continuity in function K, and gives a smoother flow profile for some problems, than $K_0 = 0$ used by Hromadka (1985). Depth $h = 0$ for dry cells. δ_s is used to bound K within finite limits; $\delta_s \approx 10^{-10}$ is used in the study for test cases in single precision. $\lambda \approx 1$ gives laminar-like flow. K is useful in linearizing and simplifying the diffusion flow equation. The continuity equation (1) can be expressed, using (6), as

$$\frac{\partial H}{\partial t} = \frac{\partial}{\partial x} K \frac{\partial H}{\partial x} + \frac{\partial}{\partial y} K \frac{\partial H}{\partial y} + S \tag{9}$$

in which $S = RF - IN - ET - q_{ea}$ is the source term. When the velocity head is included, H in (9) is replaced with E, as explained earlier. The equation can be solved for both surface flow and saturated groundwater flow using many of the methods used to solve parabolic equations.

The finite volume method

In the finite volume method (1) is expressed in the following integral form over an arbitrary control volume cv

$$\frac{\partial}{\partial t} \int_{cv} H \, dv + \int_{cv} \left[\frac{\partial}{\partial x}(hu) + \frac{\partial}{\partial y}(hv) - S \right] \, dv = 0 \tag{10}$$

in which dv = volume of element cv. The overall cv can be subdivided into cells. The Gauss divergence theorem can be used to simplify the second volume integral term of (10) and control it to a surface integral (Hirsch, 1988). Equation (10) for all the finite volume cells can be written in vector form as

$$\Delta\mathbf{A}\cdot\frac{d\mathbf{H}}{dt}=\mathbf{Q}(\mathbf{H})+\mathbf{S} \tag{11}$$

in which $\mathbf{H}=[H_1,H_2,\ldots H_m\ldots H_{nc}]^T$ is a vector containing the average heads in all the cells; $\mathbf{S}=$ the source term in vector form; $\Delta\mathbf{A}=$ a diagonal matrix whose element $\Delta\mathbf{A}(m,m)$ is equal to the cell area ΔA_m in the case of a cell m; $\mathbf{Q}$ and $\mathbf{S}$ are the net inflows and source terms to cells. The net inflow rate to a cell m is given by

$$Q_m(H)=\sum_{r=1}^{ns}(\bar{\mathbf{F}}\cdot\mathbf{n})_r\,\Delta l_r \tag{12}$$

$\Delta l_r=$ length of the side r of the ns sided polygon; $\mathbf{n}=n_x\mathbf{i}+n_y\mathbf{j}=$ unit outward normal vector for the face r of the polygon; $\bar{\mathbf{F}}=$ average flux rate across the wall per unit length defined as $hu\,\mathbf{i}+hv\,\mathbf{j}$, which is also equal to $-K\nabla H$ for free surface diffusion flow or ground water flow. Two alternative methods are used in the model to compute $\bar{\mathbf{F}}$ for overland flow. They are the line-integral-based method suggested by Hirsch (1988), and the circumcenter-based method suggested by Cordes and Putti (1996). In the case of flow over structures and levees, $Q_m(H)$ is computed using the appropriate structure equations instead of the above two methods. In the current cell-centered finite volume approach, H, ET, RF and IN are defined as cell average values.

The line-integral-based method for computing the wall flux

This method can be used with both triangular and quadrilateral cells. Using this method, the approximate flux $\bar{\mathbf{F}}_r$ for a wall r in (12) is computed by using fluxes at the nodes defining the wall. In Fig. 1,

$$\bar{\mathbf{F}}=0.5(\hat{\mathbf{F}}_j+\hat{\mathbf{F}}_k) \tag{13}$$

in which $\hat{\mathbf{F}}_j$ and $\hat{\mathbf{F}}_k$ are the fluxes at the nodes j and k computed using $-K\nabla H$. ∇H is computed using an integral equation around the nodes (Hirsch, 1988) such that

$$\int_v\nabla H\,da=\oint_s H\mathbf{n}dl \tag{14}$$

and dl = length of the sides of the polygon, referred to as the "shadow polygon", with cell centroids at vertices. Using (14), the flux $\hat{\mathbf{F}}_j$ for a node j can be expressed as

$$\hat{\mathbf{F}}_j = -K_j(\nabla\vec{H})_j = -\frac{K_j}{2\Delta\hat{A}_j}\left[-\sum_{p=1}^{np} H_p(y_{p+1}-y_{p-1})\mathbf{i} + \sum_{p=1}^{np} H_p(x_{p+1}-x_{p-1})\mathbf{j}\right] \tag{15}$$

in which $p = 1,2,\ldots,np$ are the cell numbers around the node j forming the vertices of the shadow polygon; x_p, y_p are the coordinates of these vertices. In the equation, x_0, y_0 at $p = 1$ must be replaced by x_{np}, y_{np}, and x_{np+1}, y_{np+1} at $p = np$ must be replaced by x_1, y_1 to complete the integration correctly. Areas of the shadow polygons $\Delta\hat{A}_j$ are computed by using a similar line integration:

$$2\Delta\hat{A}_j = \sum_{p=1}^{np} x_p(y_{p+1}-y_{p-1}) \tag{16}$$

K_j are computed using (7) and (8). The nodal values of n_b and h in the equations are obtained by a weighted averaging of the values of surrounding cells. The respective cell areas are used as weights. The line integrals are computed counter clockwise as positive.

In the use of the weighted implicit implementation, $\mathbf{Q}(\mathbf{H}) = [Q_1, Q_2 \ldots Q_{nc}]^T$ of (11) is linearized as $\mathbf{M}\cdot\mathbf{H}$. The matrix $\mathbf{M}$ contains information about the connectivity among cells, geometry, and the roughness. The matrix $\mathbf{M}$ is assembled by computing the flow rates across all of the walls using (12), and adding or subtracting appropriate volumes from the cells. Consider the volume lost by donor m, crossing wall r defined by nodes j and k. Equations (12), (13) and the line integral around node j obtained using (15) makes the following modification to $\mathbf{M}$:

$$M_{m,p} \rightarrow M_{m,p} - \frac{K_j\,\Delta l_r}{4\Delta\hat{A}_j}\left[-n_{xr}(y_{p+1}-y_{p-1}) + n_{yr}(x_{p+1}-x_{p-1})\right],\ p = 1,\ldots,np \tag{17}$$

n_{xr}, n_{yr} = components of $\mathbf{n}$ for wall r; Δl_r = length of wall r. A similar expression is needed for node k. Flow into the receiver cell n also requires two similar expressions with negative signs placed on (n_{xr}, n_{yr}).

The circumcenter-based method for computing wall flux

Cordes and Putti (1996) showed the equivalence of a low-order mixed finite element method based on RT0 elements (Raviart and Thomas, 1977) with a finite volume method for triangles under

certain conditions. Because of the equivalence, it is possible to use an expression derived for the mixed finite element method to compute flow rates for the finite volume method. In the equivalent finite volume method, water levels at circumcenters are used in the computation of flow across walls. In the mixed finite element method, water levels in triangles are assumed to vary linearly, and the water level at the centroid is the average water level. Using Figure 2 as the definition sketch, $(\hat{\mathbf{F}} \cdot \mathbf{n})_r$ for wall r in (12) is computed as

$$(\hat{\mathbf{F}} \cdot \mathbf{n})_r = \Delta l_r K_r \frac{H_m - H_n}{\Delta d_{mn}} \tag{18}$$

in which $\Delta d_{mn} =$ distance between circumcenters of triangles m and n; H_m, H_n are the heads at the circumcenters. K_r is computed using (7) or (8). The depth and the bed roughness needed to compute K_r are obtained by weighted averaging the depth and bed roughness of cells m and n. S_n is computed using

$$S_n = \sqrt{\frac{(\hat{H}_j - \hat{H}_k)^2}{\Delta l_r^2} + \frac{(H_m - H_n)^2}{\Delta d_{mn}^2}} \tag{19}$$

in which $\hat{H}_j$ and $\hat{H}_k$ are the heads at nodes j and k, computed as weighted averages of surrounding heads. The cell areas are used as weights in the averaging. In the semi-implicit formulation the computation of flow from cell n to m involves the modification of the following matrix element as it receives water in cell m:

$$M_{m,n} \rightarrow M_{m,n} + \frac{K_r \Delta l_r}{\Delta d_{mn}}, \qquad M_{m,m} \rightarrow M_{m,m} - \frac{K_r \Delta l_r}{\Delta d_{mn}} \tag{20}$$

Elements $M_{n,m}$, $M_{n,n}$ are modified similarly due to water losses from the donor cell n. The circumcenter-based method can be used only with acute-angled triangles. When this method is used with obtuse angled triangles, the circumcenter falls outside the triangle, and the numerical error tends to be large. With rectangles the method becomes equivalent to the finite difference method.

The average water velocity in a cell is computed by using the following vector basis function developed for RT0 mixed elements of Raviart and Thomas (1977), and used by Cordes and Putti,

(1996):

$$\vec{v} = \frac{1}{2A\,h}\left[Q_{s1}\begin{pmatrix} x-\hat{x_1} \\ y-\hat{y_1} \end{pmatrix} + Q_{s2}\begin{pmatrix} x-\hat{x_2} \\ y-\hat{y_2} \end{pmatrix} + Q_{s3}\begin{pmatrix} x-\hat{x_3} \\ y-\hat{y_3} \end{pmatrix} \right] = -K\nabla H \qquad (21)$$

Here, Q_{s1}, Q_{s2}, Q_{s3} = discharge rates across cell walls $s1, s2$ and $s3$ counting outwards as positive; $(\hat{x_i}, \hat{y_i})$ = the coordinates of the nodes; (x, y) = coordinates of any point, including the circumcenter in the current case at which the head is computed. In the case of right-angled triangles, Putti (1996) showed that the mixed finite element method is equivalent to a finite difference method.

Flow through structures and levees

When the model is used to simulate structure flows, the specific cell walls are replaced with structure type walls, and flow rates of $Q_s(H)$ are used in (12) instead of $\mathbf{F}.\mathbf{n}$ to compute structure flows. Linearization of structure flow equations can be done either prior to the run using regression methods, or during the run using data from previous calls to the routine. $Q_s(H)$ is computed as a function of adjacent water levels, gate openings, and other physical parameters. Assuming that the variation of Q_s versus ΔH $(\Delta H = H_m - H_n)$ is linear during two consecutive time steps, a structure equation can be developed using the information collected during the time steps p and $p-1$ as

$$\begin{aligned} Q_s(\Delta H) &= Q_s^p + K_s(\Delta H - \Delta H^p) \quad \text{for} \quad \Delta H^p \neq \Delta H^{p-1} \\ Q_s(\Delta H) &= Q_s^p \quad \text{otherwise} \end{aligned} \qquad (22)$$

in which $K_s = (Q_s^p - Q_s^{p-1})/(\Delta H^p - \Delta H^{p-1})$; p = the time step count. If only the information at time step p is used, (22) reduces to $Q_s(\Delta H) = K_s\,\Delta H$, and the right hand side of the system of equations need not be modified. The introduction of a structure between cells m and n modifies $\mathbf{M}$ as $M_{m,n} \rightarrow M_{m,n} + K_s$, $M_{m,m} \rightarrow M_{m,m} - K_s$, $M_{n,m} \rightarrow M_{n,m} + K_s$, and $M_{n,n} \rightarrow M_{n,n} - K_s$ as in (20). In the computations it was assumed that the head loss due to bed friction is negligible when compared to head loss across structures. If iterations are carried out within a time step, the linearization will not introduce errors in the solution. Since rapid flow variations are not expected in diffusion flow, the linearization gives good results even for structures having nonlinear flow relations.

When there is a structure or a levee type cell wall, the two-dimensional flows in adjacent cells are affected and become more nearly one dimensional. The following equation, based on the Manning equation, is applied between cells across a wall under this condition:

$$Q_{1d} = K_n \Delta H = \frac{h^{\gamma+1} \Delta l_r}{n_b \Delta d} \left(\frac{\Delta H}{\Delta d} \right)^{\lambda-1} \Delta H \tag{23}$$

Here, n_b, h are averaged between cells; $\Delta d =$ distance between the cell centroids. Centroids are used to represent cell locations in restricted spaces or closer to structures and dry cells where free 2-D flow cannot be assumed, and slope S_n of the water surface profile cannot be determined accurately. For these cells K_n is computed by assuming that the water surface slope S_n in the Manning equation is approximately equal to $\frac{\Delta H}{\Delta d}$.

Boundary conditions

One boundary condition is needed at each boundary with diffusion flow. Specified head and specified flow are the most commonly used types. The no-flow type boundary is implemented simply by making $\bar{\mathbf{F}} = \mathbf{0}$ in (12). The matrix $\mathbf{M}$ needs no modification under no-flow conditions. In the case of a known inflow rate Q_I into a cell i through the boundary or due to pumping activity, row i of source term $\mathbf{S}$ in (11) must be modified as

$$S_i \rightarrow S_i + Q_I \tag{24}$$

Source term quantities such as rainfall, ET and infiltration are summed similarly for cell i.

If the flow domain is connected to an external reservoir as the boundary condition, and if the reservoir water level is H_0, the equation for flow rate into the domain Q_o is linearized as $Q_o = K_o(H_o - H_i)$, in which K_o is similar to the structure constant K_s in (22) and H_o and H_i are water levels of the water body and the cell. The modifications for matrix $\mathbf{M}$ and vector $\mathbf{S}$ are $M_{i,i} \rightarrow M_{i,i} - K_o$, and $S_i \rightarrow S_i + K_o H_o$. Implementation of head boundary conditions is explained later.

Formulation of the weighted implicit method

The ordinary differential equations (11) derived using the finite volume method are solved by using

the following weighted finite difference formulation

$$\Delta A_i\, H_i^{n+1} = \Delta A_i\, H_i^n + \Delta t[\alpha Q_i^{n+1} + (1-\alpha) Q_i^n] + \Delta t[\alpha S_i^{n+1} + (1-\alpha) S_i^n] \tag{25}$$

in which H_i^n = average surface water level in cell i at time step n; α = time weighting factor; $\alpha = 0$ and 1 for explicit and implicit problems. Using linearization, (25) can be expressed as the following system of linear equations:

$$[\Delta \mathbf{A} - \alpha \Delta t \mathbf{M}^{n+1}].\Delta \mathbf{H} = \Delta t[\mathbf{M}^n].\mathbf{H}^n + \Delta t(1-\alpha)[\mathbf{M}^n - \mathbf{M}^{n+1}].\mathbf{H}^n + \Delta t[\alpha \mathbf{S}^{n+1} + (1-\alpha)\mathbf{S}^n] \tag{26}$$

Here, $\mathbf{Q}^n = \mathbf{M}^n.\mathbf{H}^n$. The solution $\blacksquare\mathbf{H}$ is used to update the heads using $\mathbf{H}^{n+1} = \mathbf{H}^n + \blacksquare\mathbf{H}$. The matrix $\mathbf{P} = [\Delta \mathbf{A} - \alpha \Delta t \mathbf{M}^{n+1}]$ is so far symmetric. In many gradually varying problems $\mathbf{M}^{n+1}$ is replaced with $\mathbf{M}^n$ to simplify (26) (Akan and Yen, 1981). Test runs show that this is a useful procedure for many problems. If this assumption is not made then $\mathbf{M}^{n+1}$ must be updated by using an iterative procedure within the time step, by first computing $\Delta\mathbf{H}$ using (26) with the most recent estimates of $\mathbf{M}^{n+1}$, and next updating $\mathbf{H}^{n+1}$. Iterations are continued similarly by updating $\mathbf{M}^{n+1}$ and using (26) until convergence. Examples used in the paper need only 2-4 iterations for the convergence of the water level up to 4 significant digits. This type of iteration was not used in the current application.

Imposition of a head boundary condition to a cell i as $H_i = H_B$ is carried out by reconfiguring row i of $\mathbf{P}$. The entire row i is modified by using

$$\begin{aligned} P_{i,j} &= 0 \qquad \text{for} \quad j = 1,2,\ldots nc, \quad j \neq i \\ P_{i,j} &= 1 \qquad \text{for} \quad j = 1,2,\ldots nc, \quad j = i \\ S_i &= H_B - H_i^n \end{aligned} \tag{27}$$

Matrix $\mathbf{P}$ is sparse for large problems. The element density is less than 1% for a 1000 cell discretization. When $\alpha = 0$, $\Delta\mathbf{H}$ in (26) can be computed by using a simple matrix multiplication. $\alpha = 0.5$ gives higher accuracy as in the case of Crank Nicholson type schemes. With rectangular grids the finite volume method gives the finite difference solution.

Solution of the linear equations

The number of equations in the system of linear equations in (26) is equal to the number of cells, *nc*. If the cells are non-uniform and the physical properties are non-homogeneous, the problem may become stiff and the matrix $\blacksquare\mathbf{A} - \alpha\Delta t\mathbf{M}$ may become ill-conditioned. However, many fast efficient iterative sparse solvers that can handle ill-conditioned matrices have recently become available. The current model was tested with the SLAP solver (Seager, 1988) and the PetSc solver (Smith, 1995). Both solvers use iterative conjugate gradient methods and preconditioners. Preconditioners are useful in improving the convergence rate and the solvability. Without preconditioning, the number of iterations increases with the condition number. The condition number of a matrix is the ratio of the largest and smallest eigenvalues. If the system of equations becomes difficult to solve with the choicen sparse solver, Δt can be reduced until $\mathbf{A} - \alpha\Delta t\mathbf{M}$ becomes well-conditioned. The need to re-run the code due to non-convergence can sometimes be avoided by reusing $\mathbf{M}$ with a smaller Δt.

Active research is under way to develop faster sparse solvers. A feature available with faster packages gives one the ability to solve equations at each time step as a sequential process and incrementally improve the solution by starting from the solution for the previous time step. Without such methods the same or nearly the same equations may still have to be solved repeatedly at steady or near-steady conditions, wasting computer resources. Many of the new features in solvers can make the model run much faster during such events by carrying out the minimum required updating from one time step to the next and using only a few iterations, depending on the extent of transient flow activities.

NUMERICAL TESTS

The model was tested for accuracy by applying it to a number of test problems with known solutions. The first test was used to check the ability of the finite volume method to solve diffusion equations accurately. The second test was carried out with 2-D diffusion type overland flow. The remaining tests were designed to carry out a numerical error and stability analysis.

Test 1

A groundwater example from Wang (1982) was used for the first test. In the test a pumping well was positioned at the center of a 4000 m $\times$ 4000 m square confined aquifer having a constant transmissivity ($K\times$ aquifer depth) of 300 m^2/day and a storage coefficient of 0.002. A uniform initial water level of 10 m and a constant pumping rate of 2000 m^3/s were assumed. The triangular discretization used with the model is the same as that shown later in Fig. 5 with 238 cells, except that the linear dimensions are scaled down to fit the area into the 4000 m $\times$ 4000 m square. The MODFLOW model (McDonald and Harbaugh, 1984) was set up to simulate the same flow conditions using a 40×40 square grid with 1600 cells. Figure 3a shows the water level contours at the end of 30 days, obtained by using the circumcenter-based finite volume method. Figure 3b shows the same contours obtained by using the MODFLOW model. Drawdown curves at a number of monitoring points are shown in Fig. 4. The finite volume method using the line-integral-based flow function failed to produce convex water level contours near the well, and the results are not shown. The test shows that the circumcenter-based finite volume method with only 238 cells can produce relatively accurate solutions. The test also shows that the circumcenter-based method gives better results than the line-integral-based method for locally converging flow.

Test 2

An axisymmetric overland flow problem was used in the second test. The flow characteristics of this test are somewhat similar to the flow characteristics of the Everglades. The test bed has dimensions 161 km $\times$ 161 km (100 miles $\times$ 100 miles) and a flat bottom. The initial condition is

$$H = \left[0.4575 + 0.1525\cos\left(\frac{\pi r}{r_{max}}\right)\right] m \quad \text{for} \quad r \le r_{max} \tag{28}$$

$$H = 0.305\, m \quad \text{otherwise} \tag{29}$$

in which $r =$ distance from the domain center; $r_{max} = 32188$ m. The Manning roughness is assumed as 1.0; RF, IN and ET are neglected. An axisymmetric diffusion flow model was developed based on the following axisymmetric continuity equation to obtain an extremely accurate solution for the problem using a fine resolution

$$\frac{\partial(hr)}{\partial t} + \frac{\partial(uhr)}{\partial r} = 0. \tag{30}$$

This solution was used in computing small numerical errors in the finite volume model under

different resolutions. A model, similar to the 1-D model by Akan and Yen (1981) after a few modifications, was used to solve (30) accurately. The test was a 12 day simulation of the water level using both the axisymmetric model and the finite volume model. In the test, $\Delta r = 80.47$ m and $\Delta t = 1$ min were used with the axisymmetric model to obtain the water level in the problem accurate enough to compute numerical errors in other models. The error at the center was used for comparison purposes because the error is largest at this point. The water level computed accurately at the center is 0.442105 m. The expected circular shape of the solution was also used to test accuracy of the finite volume models.

The finite volume model using the circumcenter-based approach was used with discretizations of different refinements to recreate the results of the axisymmetric model. The results, obtained using a discretization of 238 cells and 135 nodes and a time step of 3 hrs, are shown in Fig. 5. The SLAP 2.0 sparse solver package (Seager, 1988) was used to solve the linear equations, and convergence was assumed when the largest change in the solution vector $\varepsilon_\infty < 0.3 \times 10^{-4} m$. Other parameter values used were $\alpha = 0.5$ and $\delta_s = 1.0 \times 10^{-10}$ (in equations (7) and (8)). The figure shows the grid used, and the contour plot of water levels after 12 days. The water level at the center of the circular patch, and at cells at radial distances of r =11885 m and $r = 31000$ m was monitored during the simulation. Figure 6 shows the general agreement of water levels at all the monitoring points, using both the axisymmetric model and the finite volume model. Figure 6 also shows the solution at $r = 0$ obtained using a finite volume model running with a time step of 3 hrs, and a higher resolution obtained using 1536 cells. As seen in the figure, the finite volume solution very closely matches with the axisymmetric solution at this high resolution.

Numerical error and stability

The accuracy of results obtained from a numerical model depends on the spatial and temporal discretizations. If a model is used to simulate flow features of a certain wave length, the resolution of the mesh should be sufficient to capture that wave length. A description of the variation of the numerical error with the spatial and temporal resolutions is provided by Lal (1998). To understand the behavior of the numerical error in the current finite volume model, triangular meshes of dif-

ferent levels of discretization were used in the simulation of the flow pattern used in the previous test case. The GMS software package (1995) was used to generate meshes for this test. An estimate of the numerical error was obtained for comparison purposes by presenting the numerical error at $r = 0$ after 12 days as a percentage of the depth at $t = 0$. Numerical error was computed by using the previously mentioned axisymmetric solution as the true solution because it has an error term much smaller than the error studied. Table 1 shows a summary of test results for the center, obtained by using circumcenter-based methods. Run times shown are for a SUN Sparc 20 (speed 90 MHz, 4.1 Mflops/s measured with the linpack benchmark test, Dongarra, 1993). The iterations shown are the iterations inside the SLAP2.0 solver indicating the computational effort. In the table Δx was computed as $\sqrt{\Delta A_c}$ in which ΔA_c is the average area of a triangular cell. ϕ is obtained as $k\Delta x$, in which k is the wave number of the water surface profile simulated in the model $= 2\pi/(\text{wavelength})$. Term π/ϕ gives an estimate of the spatial resolution, measured as the average number of spatial divisions within half the wave length of a sinusoidal water surface profile. β is the non-dimensional time step size, which is based on the analysis of Lal (1998):

$$\beta = \frac{h^{\frac{5}{3}}}{n_b\sqrt{S_n}}\frac{\Delta t}{\Delta x^2} \tag{31}$$

$\beta < 0.25$ for explicit finite difference methods. Test 0 corresponds to the test shown in Figures 5 and 6 for 238 cells. Results of test 12 with 1536 cells is also shown in Fig 6. Table 1 shows that the solution of the finite volume model approaches the axisymmetric solution as the spatial and temporal resolutions both get finer. This is true when the model is using the line-integral-based method too. Table 1 also shows that the run time decreases and the number of iterations per time step increases when the time step is increased.

A test was conducted to check the stability of the model under explicit conditions ($\alpha = 0$). Experimentation with different time steps showed that Δt at the points of incipient instability of the tests was approximately 52 hrs, 4.3 hrs and 3.5 hrs respectively with 116, 376 and 1536 cell configurations listed in Table 1. These time steps correspond to approximate β values of 0.06, 0.02 and 0.05 respectively. Incipient instability was assumed when dynamic oscillations were visible at the center of the solution. These results confirm, for example, that the tests 8-11 in Table 1, ob-

tained for $\alpha = 0.5$, would have been unstable under explicit conditions. The approximate stability limit $\beta \approx 0.05$ is useful in selecting the time step for explicit model runs. Nonlinear instability was not studied during the test.

Numerical tests were conducted to determine the convergence behavior of the finite volume code and the influence of δ_s in (8) on the performance of the code. Tests showed that the number of iterations increased when δ_s was decreased to very low values, because some of the K values in the matrix became very large (Lal et al., 1997), and the matrix became more unconditional and ultimately unsolvable as a result. The solution errors at the center after 12 hrs were 1 mm, 21 mm, and 88 mm as δ_s was changed to 10^{-6}, 10^{-5} and 10^{-4} respectively. A large δ_s causes the model to use (8) instead of (7) more often. $\delta_s = 10^{-10}$ was used in the axisymmetric flow test, and $\delta_s = 10^{-4}$ was used in the Kissimmee study that is explained later.

Different sparse solver options in the SLAP 2.0 package were tested while running test 0 referred to in Table 1. The purpose of the test was to investigate the performance of different solvers and pre-conditions. In the SLAP 2.0 package the incomplete LU decomposition with conjugate gradient (CG) solver, incomplete LU biconjugate gradient solver, and the incomplete LU biconjugate gradient solver with LU decomposition were reliable, and used the least number of iterations. The last option was used in the test. The number of solver iterations changed with the solver type and δ_s which affects the condition number of the matrix. With large time steps the SLAP 2.0 solver converged only when large α values are used. The recently developed PetSc solver (Smith et al., 1995) was found to be much more reliable and fast for larger problems.

Application to the Kissimmee River

The model was applied to the an experimental area near weir no. 2 of the Kissimmee River Basin, Florida, using the same discretization and the bed roughness used by Zhao et al. (1994). In the application by Zhao et al. the unsteady flow model RBFVM-2D was used over the test area shown in Fig. 7, which is approximately 1402 m $\times$ 1036 m. In the figure a flood canal passes from the

North to the South (left to right in the figure), and a one-notch weir is located near the upstream end near C1 to divert part of the flow into the river oxbow. The Manning coefficients of the flood plain, main channel and the river oxbow are 0.03, 0.025 and 0.04 respectively. The number of nodes and cells in the mixed grid used by the RBFVM-2D model and the line-integral-based finite volume model are 347 and 327 respectively. The same numbers in the case of the circumcenter-based method are 347 and 634 respectively. For the circumcenter-based method the quadrilaterals were divided into triangles. The results of the problem for an inflow of 221 m^3/s at the upstream boundary and a stage of 13.57 m at the downstream boundary are shown in Fig 7, after running the model until a reasonably steady state is reached. The results were obtained after including the velocity head $V^2/(2g)$ in (5). When the same simulation was repeated with the omission of the velocity head, the water level at C1 dropped by 1 cm. Water levels at other locations remained practically unchanged. Figure 7 shows contours of water levels, and the water level monitoring points. The elliptical patch of contours in the figure shows a small dry area. Figure 8 shows the velocity vectors drawn at the circumcenters using (21). The apparent overlap of arrows in the plot is due to the near right-angled triangles in the grid, which make the circumcenters nearly overlap. Figure 9 shows the results of the same test obtained using the line-integral-based method.

Comparison of water levels and water velocities in Table 2 shows that the water levels obtained with the current model agree with the physical model results and the RBFVM-2D model results at many locations. However velocities at O2, representing a narrow canal segment of the Oxbow, that were obtained by using diffusion flow models did not agree with other velocities. Comparison of the circumcenter-based method with the line-integral-based method show that both methods produced similar flow patterns in the Kissimmee application, unlike in the test cases with a locally convergent or divergent flow fields in which the line-integral-based method produced unacceptable local results. This occurred because the averaged $\bar{\mathbf{F}}$ in (13) does not provide a very accurate estimate of discharges across walls in acute angled triangles. Certain velocities near the boundary are not shown in Table 2 because line integrals could not be computed with this method without a closed path of integration.

With the Kissimmee application it was also found that the line-integral-based method required approximately 50 iterations when using 20 s time steps and the SLAP conjugate gradient method using LU decomposition preconditioner. The circumcenter method required approximately 200 iterations for the same case. The run time for the current model is a small fraction of the run time of explicit models such as RBFVM2D requiring 1-2 s time steps. The PetSc solver (Smith, 1995) with a new C++ version of the current model can reduce the number of iterations to less than 5 with even larger time steps, and make the model run much faster. With the development of better and faster external sparse solvers using parallel processing and other methods, large scale application of the model to South Florida continues to become less expensive, just with the upgrading of the solver.

SUMMARY AND CONCLUSIONS

An implicit finite volume model was developed to simulate diffusion flow across arbitrarily shaped landscapes. Tests were conducted to verify the model results by comparing them with results from the MODFLOW model and an axisymmetric model. The model was also applied to a variety of test problems, using a range of spatial and temporal discretizations to study the behavior of numerical errors. Results show that numerical errors tend to become smaller with finer discretizations, thus confirming the numerical consistency condition. The explicit option ($\alpha = 0.0$) showed incipient instability when the non-dimensional time step β exceeds approximately 0.05. The implicit option was stable for large values of β. Results show that, by selecting a spatial resolution (π/ϕ) of more than about 3 divisions per half sine wave, numerical errors for the test problems can be reduced to less that 1%.

The model used different wall types to represent structure flows, no flows, and 2-D flows. Flow across 2-D walls were computed by using a line-integral-based method and a circumcenter-based method. Results show that the circumcenter-based method produced better results under all the conditions tested, and that the line-integral-based methods produced local errors when used

with triangular discretizations to simulate locally convergent or divergent flow patterns. The line-integral-based method becomes the choice when polygons, not triangles, are used in the discretization. This method also needed fewer iterations inside the solver when used with test problems. Application of both methods to the Kissimmee River shows that the results agree with the results of the physical model and the RBFVM-2D model. The same application showed that, while the RBFVM-2D model needed 1-2 s time steps, the current model could be run faster with time steps over 10 times as large, even with older solvers, and many more times faster with modern solvers.

The structure of the current finite volume model allows new wall flow function types to be added to the existing circumcenter and line integral types, and new structure types to be added in the same way. This feature is useful for future extensions of the model into more complicated areas of South Florida and the Everglades. Increasingly powerful sparse solvers can continue to speed computations in the future and make it possible to simulate flows with much finer spatial resolutions and larger time steps otherwise possible, as demonstrated in the examples.

ACKNOWLEDGEMENTS

The writer wishes to thank Mark Belnap, Randy Van Zee, and Jayantha Obeysekara for providing valuable ideas during different stages of model development. Review of the manuscript by Todd Tisdale, Joel VanArmen, Steve Lin, Brion Lehar, Sashi Nair, Mark Wilsnack, and other members of the Hydrologic Systems Modeling group of the South Florida Water Management District was extremely useful.

APPENDIX I. REFERENCES

Abbott, M. B. (1979). *Computational hydraulics*, Ashgate Publishing Co., Brookfield, USA.

Akan, A. O., and Yen, B. C. (1981). "Diffusion-wave flood routing in channel networks", *J. Hydr. Div.,* ASCE, 107(6), 719-731.

Akanbi, A. A., and Katopodes, N. D. (1988). "Models for flood propagation on initially dry land", *J. Hydr. Engrg.,* ASCE, 114(7), 686-706.

Aziz, K. and Settari, A. (1979). *Petroleum Reservoir Simulation*, Elsevier Publishing Co., NY.

Barrett, R., Berry, M., Chan, T., Demmel, J., Donato, J., Dongarra, J., Eijkhout, V., Pozo, R., Romine, C., and van der Vorst, H. (1993). "Templates for the solution of linear systems: building blocks for iterative methods", *SIAM Publications, 1993*, distributed through `ftp netlib2.cs.utk.edu`.

Chaudhry, M. F. (1993). *Open-Channel Flow*, Prentice-Hall, NY.

Chow, V. T., and Ben-Zvi, A. (1973). "Hydrodynamic modeling of two-dimensional water flow", *J. Hydr. Div., ASCE*, 99(11), 2023-2040.

Cordes, C., and Putti, M. (1996). "Triangular mixed finite elements versus the finite volumes in groundwater modeling", Int. Conf. Comp. Meth. Water Res. XII, A. A. Aldama et al., editors, *Computational Mechanics*, Southampton, London, p 61-68.

Dongarra, J. (1993). "Performance of various computers using standard linear equation software", Computer Science Dept., Univ. of Tennessee, CS-89-85.

Dongarra, J., Lumsdaine, A., Pozo, R., and Remington, K. (1995). "IML++ v. 1.1. Iterative methods library", *National Institute of Standards and Technology Report, February 1995*, University of Tennessee, TN.

Fennema, R. J., and Chaudhry, M. H. (1990). "Explicit methods for 2D transient free-surface flows", *J. Hydr. Engrg.,* ASCE, 116(8), 1013-1034.

Fennema, R. J., Neidrauer, C. J., Johnson, R. A., McVicor, T. K., Perkins, W. A. (1994). "A computer model to simulate natural everglades hydrology", *Everglades, The Ecosystem and its Restoration,* Eds. Davis, S. M. and Ogden, J. C., St. Lucie Press, FL, 249-289.

Fenner, R. T. (1975). *Finite element method for engineers*, MacMillan, London.

Fread, D. L. (1973). ”Effects of time step in implicit dynamic routing”, *Water Resources Bulletin*, AWRA, 9(2), 338-350.

Fread, D. L. (1988). ”The NWS DAMBRK Model”, *National Weather Service*, NOAA, Silver Springs, MD.

Garcia, R. and Kahawita, R. A. (1986). ”Numerical solution of the St. Venant equations with the McCormack finite difference scheme.”, *Int. J. Numerical Methods in Fluids*, Vol. 6, 507-527.

GMS Department of Defence Groundwater Modeling System. (1995). Computer Graphics Laboratory, Bringham Young University, UT.

Hirsch, C. (1988). ”Numerical computation of internal and external flows”, *John Wiley & Sons,* New York.

Hromadka, II, T. V. and Lai, C. (1985). ”Solving the two-dimensional diffusion flow equations”, *Proc. of the specialty conf. sponsored by the Hyd. Div. of the ASCE*, lake Buena Vista, FL, Aug 12-17, 555-561.

Hromadka II, T. V., McCuen, R. H., and Yen, C. C. (1987). ”Comparison of overland flow hydrograph models”, *J. of Hydr. Res.,* ASCE, 113(11), 1422-1440.

Kadlec, R. H. and Knight, R. L. (1996). *Treatment wetlands*, Lewis Publishers, Boca Raton, FL, 197-207.

Katopodes, N. D., and Strelkoff, R., ”Computing two-dimensional dam break flood waves”, *J. Hydr. Div., ASCE*, 104(9), 1269-1288.

Lal, Wasantha, A. M. (1998). ”Performance comparison of overland flow algorithms”, *J. of Hydr. Engrg.,* ASCE, 124(4).

Lal, Wasantha, A. M., Belnap, M. (1997). ”A users guide to HSE, the hydrologic simulation engine of the South Florida Regional Simulation Model”, South Florida Water Management District, West Palm Beach, FL.

Liggett, J. A. and Woolhiser, D. A. (1967). ”Difference solutions of the shallow-water equation” *J. Eng. Mech. Div.*, ASCE, 93(2), 39-71.

McDonald, M. and Harbaugh, A. (1984). ”A modular three dimensional finite difference ground-water flow model”, *US Geological Survey*, Reston, VA.

Ponce, V. M., Li, Ruh-Ming, Simons, D. B. (1978). ”Applicability of Kinematic and diffusion models”, *J. Hydr. Engrg.,* ASCE, 104(3), 353-360.

Panton, R. L. (1984). ”Incompressible Flow”, *John & Wiley Sons*, NY, 315-316

Raviart, P. A. and Thomas, J. M. (1977). ”A mixed finite element method for second order elliptic problems”, in Galligani, I., and Magenes, E., editors, *Mathematical aspects of the finite element method*, Springer-Verlag, New York.

Seager, M. L. (1988). ”SLAP, Sparse linear algebra package 2.0”, based on the report ”Routines for solving large sparse linear systems”, *Lawrence Livermore National lab*, Livermore Computing Center, January 1986 Tentacle pp 15-21.

Smith, B. F., McInne, L. C. and Gropp, W. D. (1995). *PETSc 2.0 user manual*, Tech Rep. ANL-95/11, Argonne National Lab.

Strelkoff, T., Schamber, D., and Katopodes, N. (1977). ”Comparative analysis of routing techniques for the flood wave from a ruptured dam”, *Proceedings of Dam-Break Flood-Routing-Model Workshop held in Bethesda, MD*, held on Oct., 18-20, 1977. Sponsored by Water Resources Council. U. S. Dept. of Commerce, NTIS, PB-275 437, pp 227-291.

Tan, Weyyan. (1992). *Shallow water hydrodynamics*, Elsevier Publishing Co., NY.

Wang, Herbert. (1982). *Introduction to groundwater modeling*, W. H. Freeman Co. NY.

Xanthopoulos, T. and Koutitas, C. (1976). ”Numerical simulation of a two-dimensional flood wave propagation due to dam failure”, *Journal of Hydraulic Research*, 14 (4), 321-331.

Zhao, D. H., Shen, H. W., Tabios III, G. Q., Lai, J. S., and Tan, W. Y., (1994) ”Finite-volume two-Dimensional unsteady-flow model for river basins”, *J. Hydr. Engg.,* ASCE, 120(7), 863-883.

DEFINITION OF VARIABLES

Variable	Definition
E	energy head (m).
$\bar{\mathbf{F}}_r$	average flux vector across the wall r.
$\hat{\mathbf{F}}_k$	flux vector at a node k.
g	gravitational acceleration.
$\mathbf{H}$	average water levels of all the cells, in vector form (m).
$\hat{H}$	water levels at the nodes (m).
h	depth of water (m).
K	hydraulic conductivity (m/s).
$\mathbf{M}$	matrix obtained after linearizing $\mathbf{Q}$.
$\mathbf{n}$	unit normal to a wall.
n_b	Manning roughness coefficient.
$\mathbf{Q}(\mathbf{H})$	inflow into all the cells, in vector form.
Q_s	flow rate across a structure.
$\mathbf{S}$	source or sink terms for all the cells, in a vector form.
$\vec{S}_f$	friction slope vector.
S_n	slope of the water surface or the energy surface.
$\mathbf{V}$	flow velocity vector.
u, v	x and y components of flow velocity (m/s).
x,y	space coordinates (m).
$\hat{x}$,$\hat{y}$	nodal coordinates.
z	ground elevation above datum (m).
$\Delta\mathbf{A}$	a diagonal matrix with the cell areas at the diagonals.
ΔA_i	area of cell i

Variable	Definition
$\Delta\hat{A}_i$	area of shadow cell i
Δd_{mn}	distance between circumcenters of triangles m and n.
Δl_r	length of wall r.
δ_s	slope below which only an approximate Manning eq. is used.
Δt	time step (s).

Table 1: Solutions of the test problems using various discretizations. Results of test 0 with non-homogeneous cells are shown in Figs 5 and 6. CPU is an abbreviation for central processing unit time.

Test	No. elem.	No. nodes	CPU (s)	No. iter.	Δx (m)	Δt (s)	h_{end} (m)	π/ϕ	β	ε %
1	116	69	2.4	18	14939	51840	0.4488	2.15	0.016	1.09
2	116	69	8.8	12	14939	10368	0.4484	2.15	0.003	1.03
3	116	69	16.4	11	14939	5184	0.4484	2.15	0.002	1.02
4	376	209	6.0	40	8298	207360	0.4450	3.88	0.212	0.48
5	376	209	25.1	19	8298	20736	0.4446	3.88	0.021	0.40
6	376	209	43.6	17	8298	10368	0.4444	3.88	0.011	0.38
7	376	209	78.8	13	8298	5184	0.4444	3.88	0.005	0.37
8	1536	809	60.1	104	4105	518400	0.4540	7.84	2.166	1.96
9	1536	809	75.3	78	4105	207360	0.4449	7.84	0.866	0.48
10	1536	809	98.3	67	4105	103680	0.4450	7.84	0.433	0.48
11	1536	809	258.0	35	4105	20736	0.4439	7.84	0.087	0.29
12	1536	809	436.0	27	4105	10368	0.4437	7.84	0.043	0.27
0	238	135	27.7	1	10429	5184	0.4390		0.50	0.49

Table 2: Comparison of physical model results with the results of the finite volume models using circumcenter-based walls and line-integral-based walls. Results of the finite RBFVM-2D model by Zhao et al. (1994) are also shown.

Gage	Physical model		RBFVM-2D model		Circum. meth.		Line int. Meth.	
	Velocity m/s	Stage m	Velocity m/s	Stage m	Velocity m/s	Stage m	Velocity m/s	Stage m
C1	0.30	13.87	0.29	13.78	0.24	13.87	–	13.85
C3	0.23	13.57	0.21	13.60	0.26	13.66	–	13.62
C4	0.23	13.57	0.25	13.60	0.25	13.61	0.28	13.61
C5	0.23	13.57	0.29	13.57	0.25	13.60	0.29	13.59
C6	0.23	13.57	0.31	13.58	0.27	13.57	0.27	13.58
C7	0.29	13.57	0.33	13.69	0.21	13.57	–	13.57
O1	0.85	13.67	0.67	13.69	0.98	13.77	0.70	13.73
O2	0.49	13.67	0.44	13.64	0.06	13.60	0.14	13.64

LIST OF FIGURES

Fig. 1: A diagram showing the definition of variables used in the line integral method.

Fig. 2: A diagram showing the definition of variables used in the circumcenter method.

Fig. 3 a: Drawdown contours obtained using the finite volume model.

Fig. 3 b: Drawdown contours obtained using the MODFLOW model.

Fig. 4: Variation of drawdown with time at different distances.

Fig. 5: A contour plot of the water levels in the axisymmetric test problem.

Fig. 6: Variation of the water level with time in the axisymmetric test problem.

Fig. 7: A contour plot of the water levels in the Kissimmee river, obtained using the circumcenter method.

Fig. 8: A vector plot of the water velocities in the Kissimmee river obtained using the circumcenter-based walls.

Fig. 9: A contour plot of the water levels in the Kissimmee river, obtained using the line-integral-based walls.

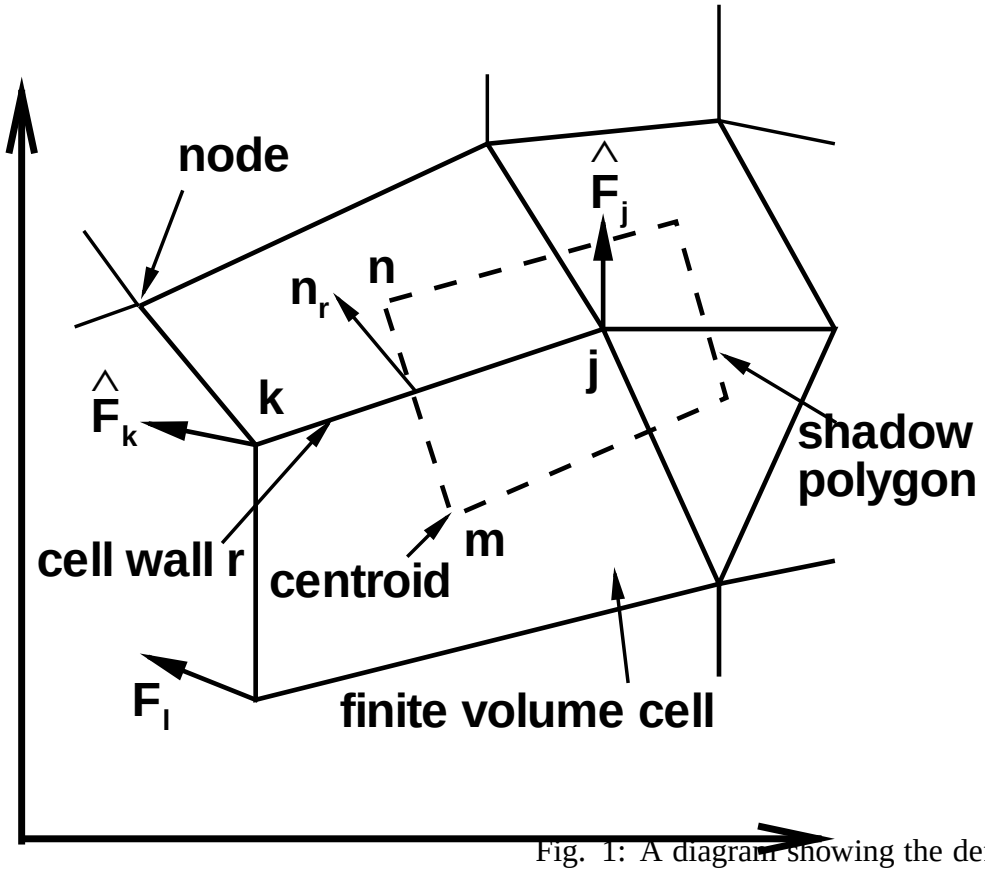

Fig. 1: A diagram showing the definition of variables used in the line integral method.

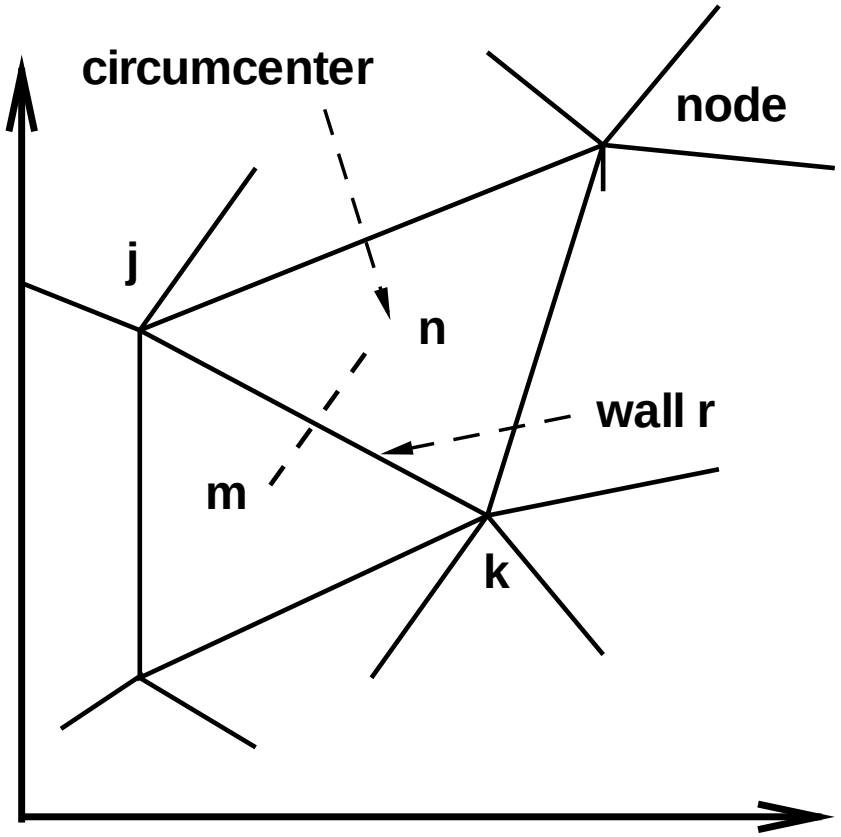

Fig. 2: A diagram showing the definition of variables used in the circumcenter method.

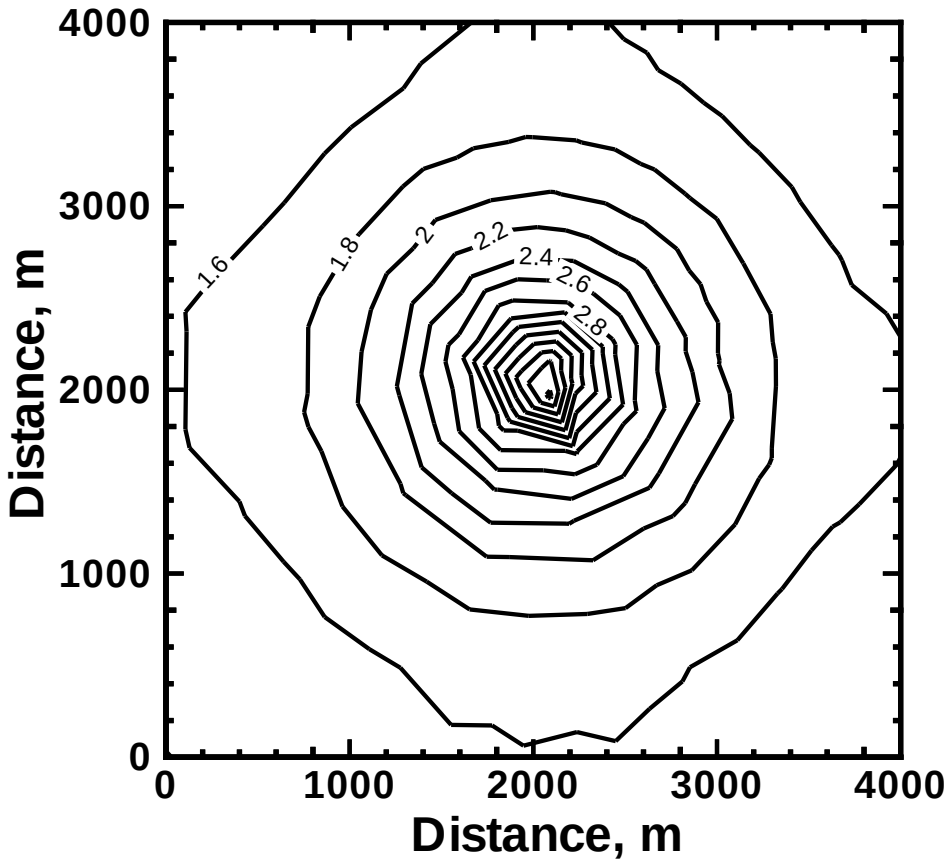

Fig. 3 a: Drawdown contours obtained using the finite volume model.

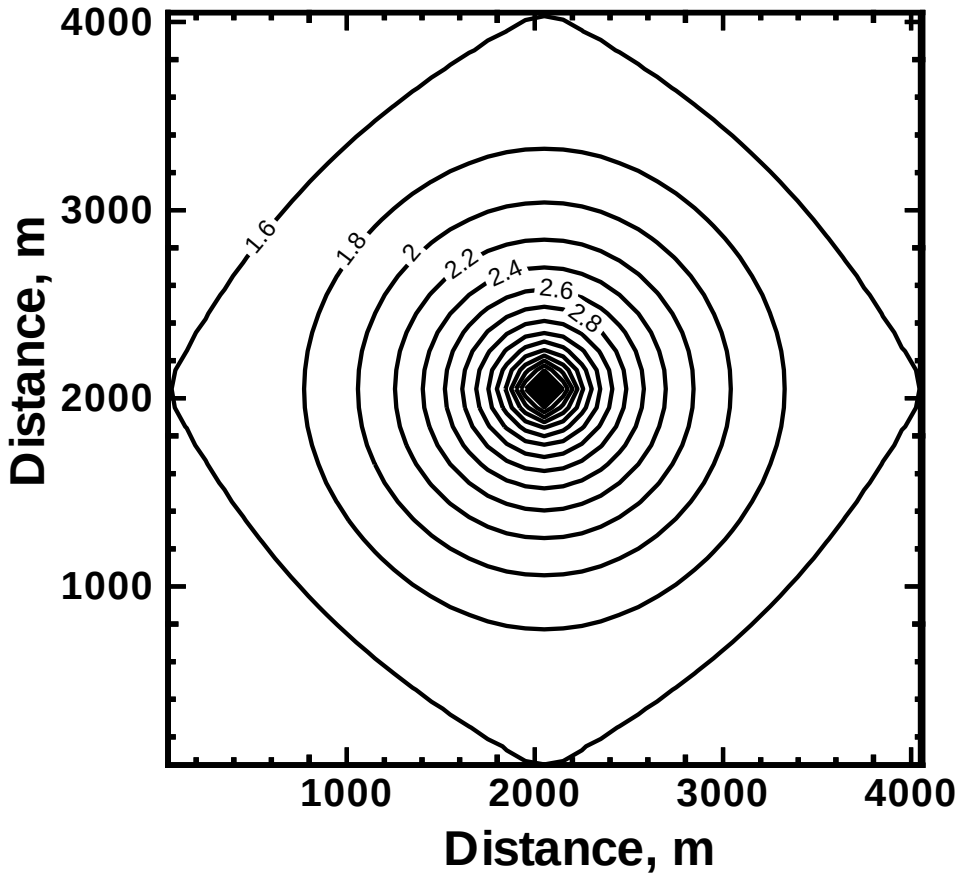

Fig. 3 b: Drawdown contours obtained using the MODFLOW model.

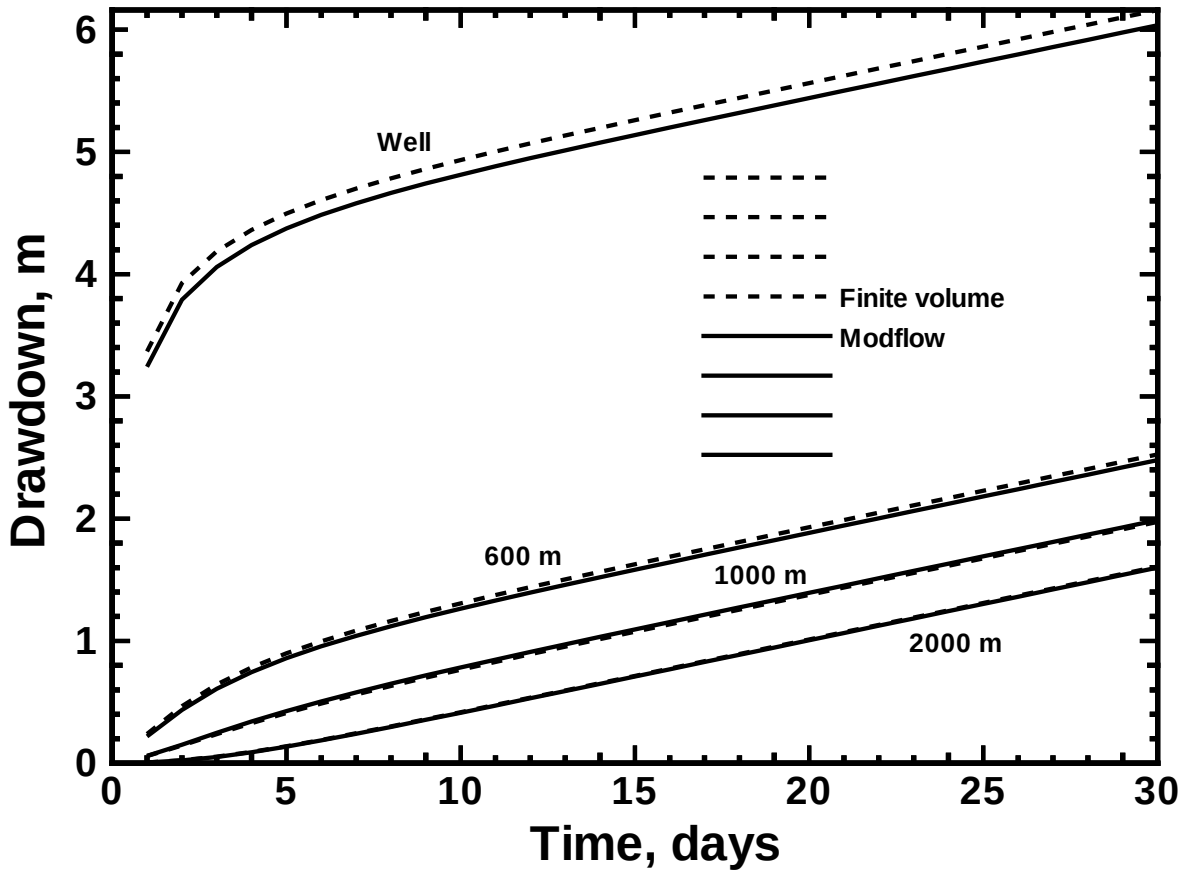

Fig. 4: Variation of drawdown with time at different distances.

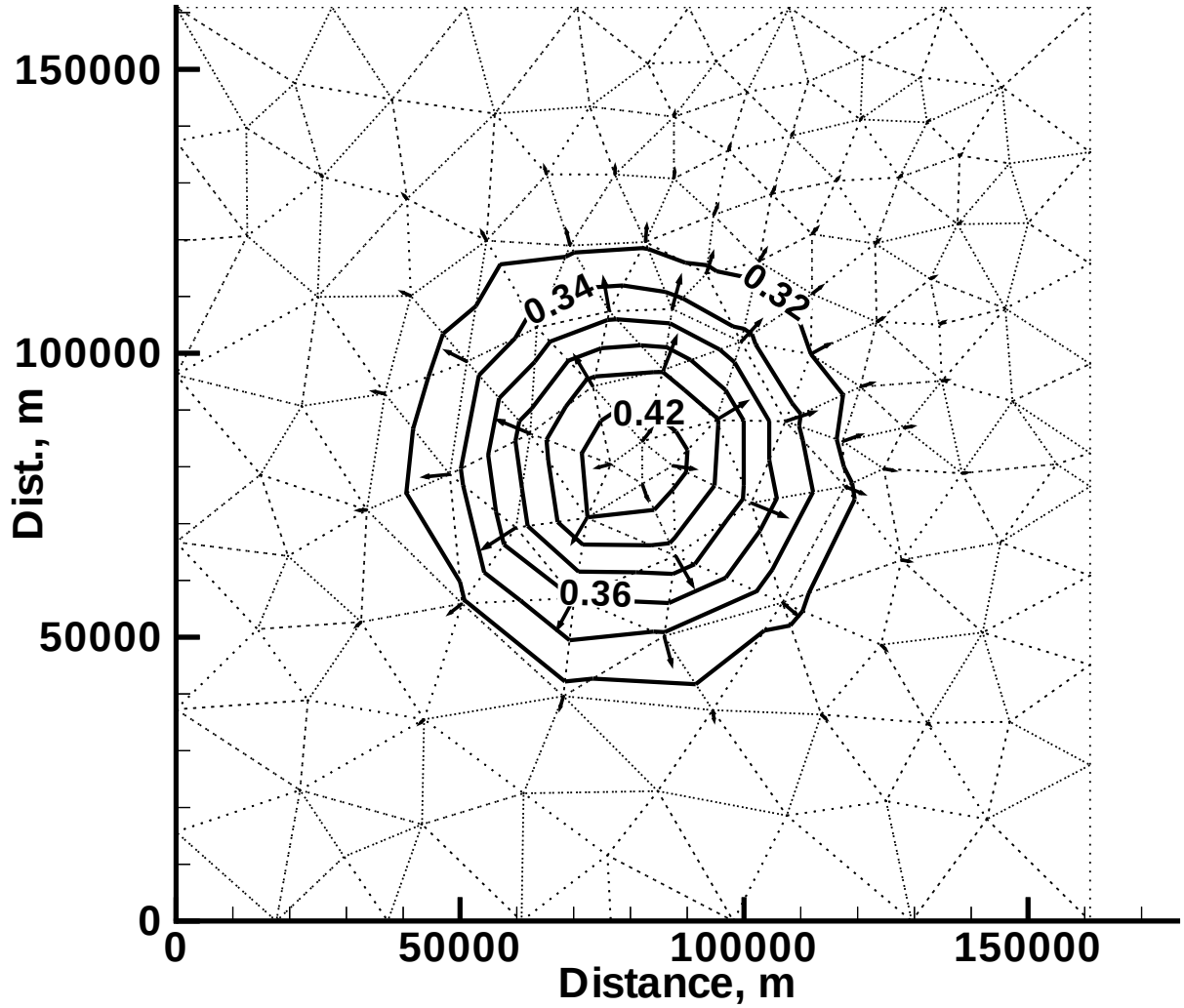

Fig. 5: A contour plot of the water levels in the axisymmetric test problem.

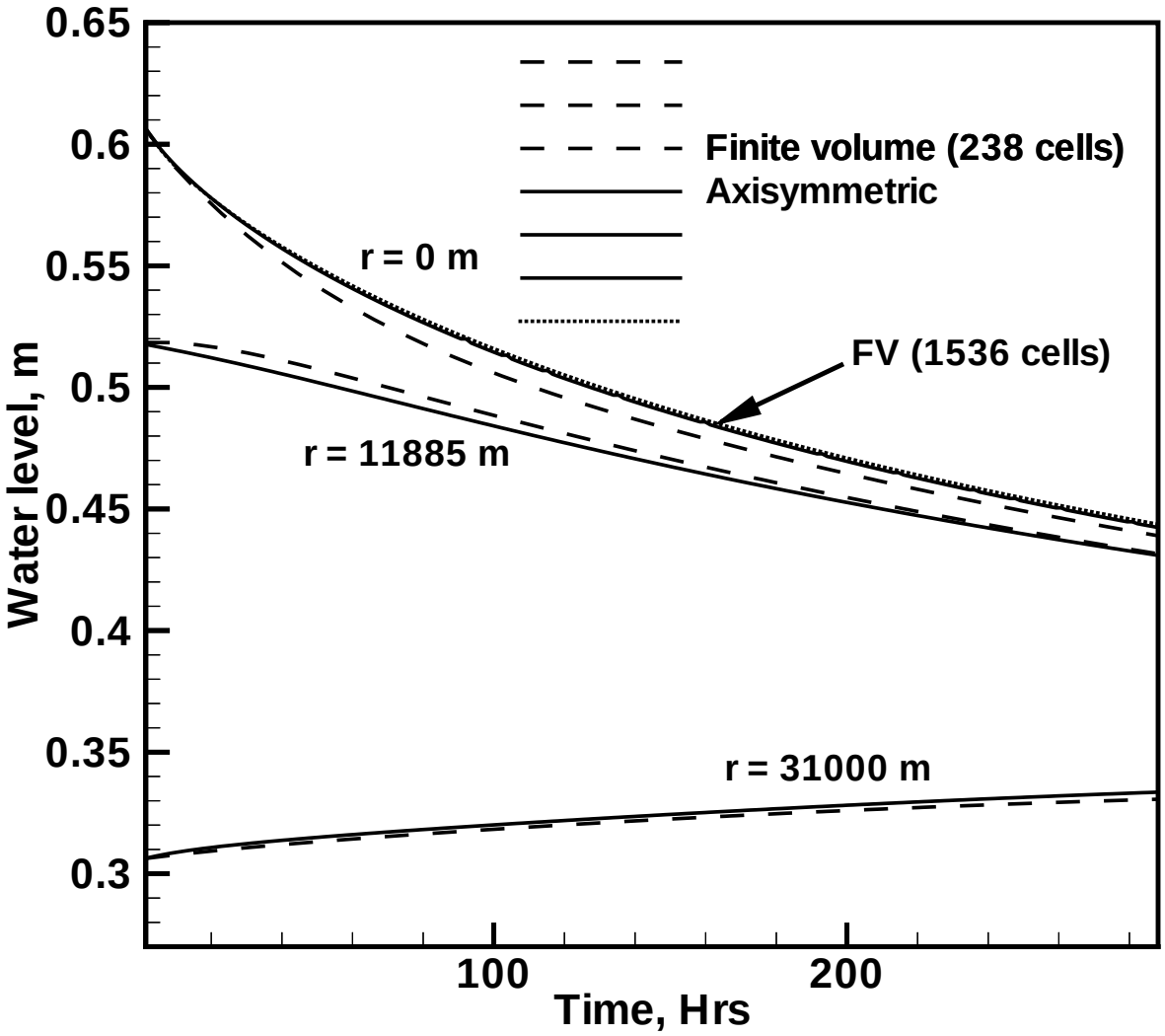

Fig. 6: Variation of the water level with time in the axisymmetric test problem.

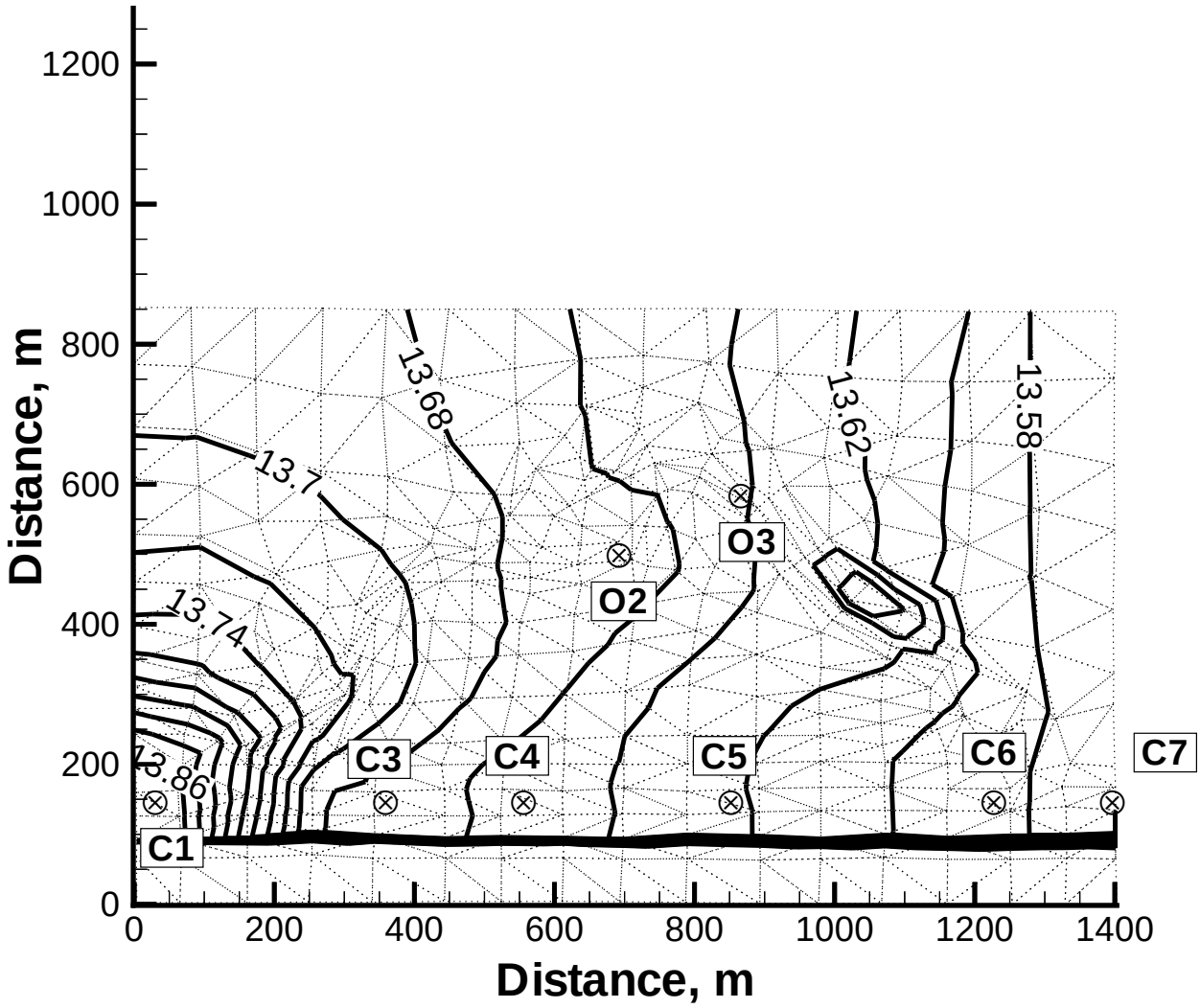

Fig. 7: A contour plot of the water levels in the Kissimmee river, obtained using the circumcenter method

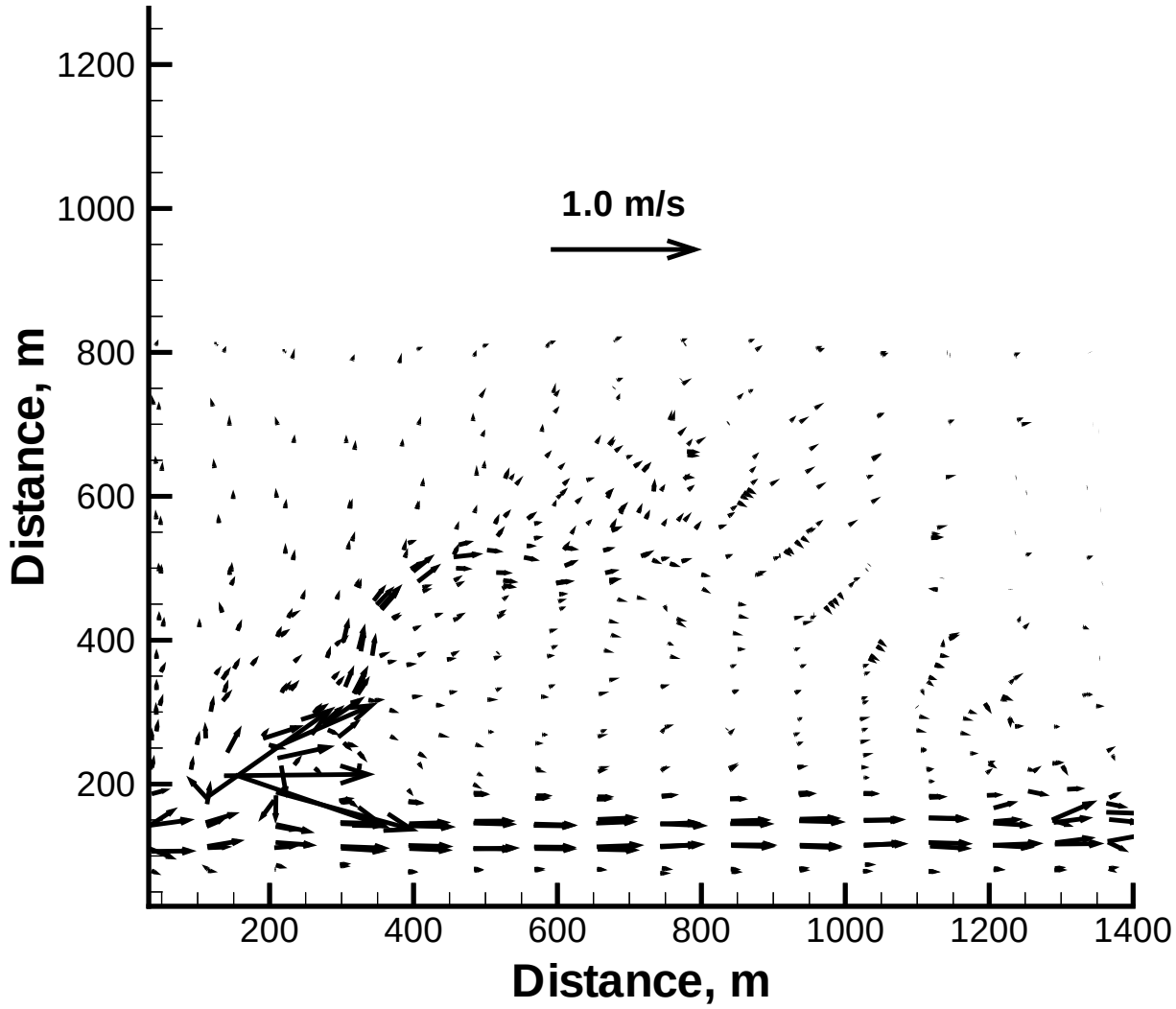

Fig. 8: A vector plot of the water velocities in the Kissimmee river obtained using the circumcenter-based walls.

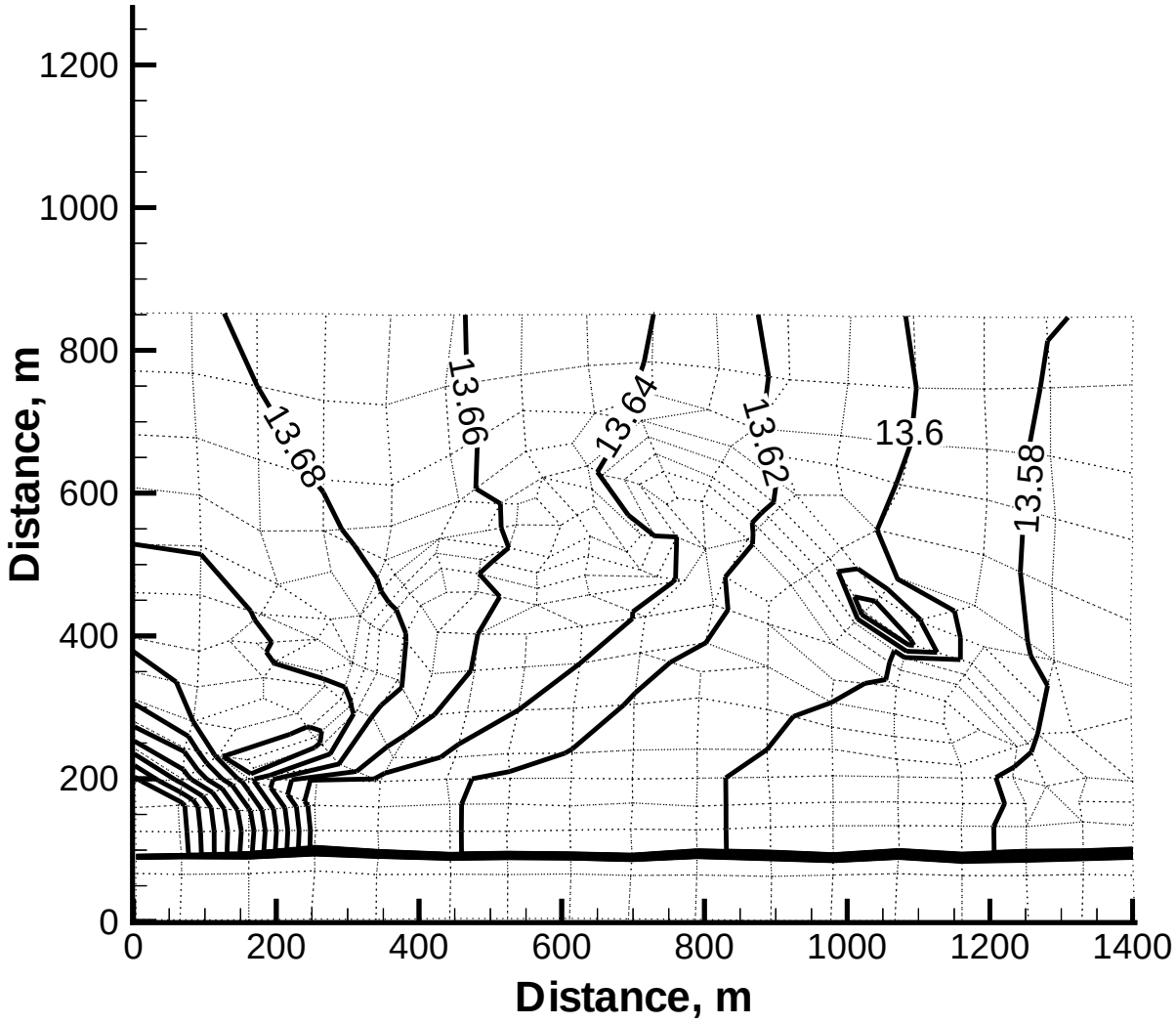

Fig. 9: A contour plot of the water levels in the Kissimmee river, obtained using the line-integral-based walls.